SvedbergOpen
DISSEMINATION OF KNOWLEDGE

International Journal of Artificial Intelligence and Machine Learning

Publisher's Home Page: https://www.svedbergopen.com/

Research Paper Open Access

Deep Learning for Prostate Cancer Diagnosis Using Computed Tomography: A comprehensive Review of CNN Architectures, Clinical Applications, Challenges, and Future Directions

B. Manju[1], J. Asha[2], Soumya Varma[3], Ajay James[4*]

[1]Professor, Department of Electrical and Electronics Engineering, Affiliated to A.P.J. Abdul Kalam Kerala Technological University, Government Engineering College, Thrissur- 680009.
[2]Associate Professor, Department of Electronics and Communication Engineering, Affiliated to A.P.J. Abdul Kalam Kerala Technological University, Government Engineering College, Thrissur- 680009.
[3]Department of CSE, Karunya Institute of Science and Technology, Coimbatore, Tamil Nadu.
[4*]Associate Professor, Department of Computer Science and Engineering, Affiliated to A.P.J. Abdul Kalam Kerala Technological University, Government Engineering College, Idukki. E-mail : ajay@gectcr.ac.in

ABSTRACT
Prostate cancer is one of the most common malignancies and a leading cause of cancer-related death among men worldwide. Although magnetic resonance imaging and prostate-specific membrane antigen positron emission tomography/computed tomography are central to prostate cancer diagnosis and staging, computed tomography remains widely accessible and important for staging and radiotherapy planning, particularly in resource-limited settings. This review critically examines convolutional neural network applications in prostate computed tomography imaging and compares them with evidence from magnetic resonance imaging, positron emission tomography/computed tomography, and ultrasound. We conducted a structured narrative review of relevant literature published between 2021 and 2026, supplemented by seminal studies on established convolutional neural network architectures. The review identified a clear imbalance in current applications: computed tomography research predominantly focuses on automated segmentation of the prostate and surrounding organs for radiotherapy planning and on lesion segmentation in positron emission tomography/computed tomography, whereas direct diagnostic classification remains comparatively limited. Reported segmentation performance is generally strong, whereas diagnostic classification studies are smaller and more heterogeneous. Explainable artificial intelligence methods may improve model interpretability, although their reliability remains variable. Future progress requires larger multicentre datasets linked to histopathology, standardized performance reporting, rigorous external validation, and the integration of computed tomography-based models as adjuncts rather than replacements for established diagnostic pathways.

Keywords: Prostate Cancer, Computed Tomography, Convolutional Neural Networks, Deep Learning, Radiomics, And Explainable Artificial Intelligence

Introduction

Prostate cancer (PCa) is the second most common cancer diagnosed and a leading cause of cancer-related death among men worldwide. Its incidence is especially increasing in areas experiencing rapid gains in life expectancy and access to diagnostics [1-3]. The disease's progression varies widely, from slow-growing, low-grade cases suitable for active surveillance to aggressive, metastatic forms that need multimodal treatment. This heterogeneity underscores the importance of precise, consistent, and early diagnostic assessment.

Conventional diagnostic pathways combine serum prostate-specific antigen (PSA) testing, digital rectal examination, and, when PSA levels or clinical findings are suspicious, systematic or MRI-targeted transrectal biopsy [75]. Multiparametric MRI (mpMRI) has become the imaging backbone of the modern PCa diagnostic pathway, supported by trials demonstrating its superiority over systematic biopsy alone in detecting clinically significant disease [75]. PSMA PET/CT has separately established itself for staging and biochemical recurrence. By contrast, plain or contrast-enhanced CT occupies a narrower but persistent clinical niche: it is inexpensive, fast, widely available even in resource-constrained settings, and forms the anatomical backbone of radiotherapy treatment planning, where the prostate and surrounding organs at risk (bladder, rectum, femoral heads) must be delineated for every fraction of external-beam therapy. A key challenge in using CT for prostate cancer diagnosis lies in its limited soft-tissue contrast compared to MRI. As a result, the prostate gland and any intraglandular lesions often appear indistinguishable on non-contrast images [16]. This physical limitation largely shapes the existing literature: research with convolutional neural networks (CNNS) mainly focuses on segmenting organs and target volumes for radiotherapy and on PSMA PET/CT lesion segmentation and staging- where the PET signal provides the diagnostic information- rather than detecting primary lesions from CT alone.

Since Alexnet's breakthrough in natural image classification [59], CNNS have rapidly progressed, propelled by

architectural innovations like residual connections [56], dense connectivity [57], attention mechanisms, and more recently, vision transformers [67,68]. These advances have steadily narrowed the performance gap between handcrafted radiomic features and learned deep representations. In CT imaging, such architectures now underpin top auto-segmentation tools like nnU-Net [70], which are routinely employed in some radiotherapy clinics. Moreover, their use is cautiously expanding into CT-based diagnostic classification and risk assessment.

This review critically analyses convolutional neural network architectures used in prostate imaging, focusing on computed tomography and related modalities such as prostate-specific membrane antigen PET/CT and cone-beam CT. It also compiles and compares public datasets pertinent to deep learning in prostate CT and MRI research. Additionally, the review evaluates quantitative performance data across CT, PET/CT, MRI, and ultrasound studies to assess the clinical utility of CT and identify areas where other modalities outperform it. The role of explainable AI in clinical decision-making is also considered. Lastly, it discusses methodological, regulatory, and ethical challenges that hinder clinical adoption and suggests key directions for future research.

2. Background

2.1 Prostate Anatomy

The prostate is a small, walnut-sized exocrine gland located below the bladder and in front of the rectum. It is typically divided into peripheral, transition, and central zones according to Mcneal's zonal anatomy, with most adenocarcinomas arising in the peripheral zone. This zonal structure is clearly visible on T2-weighted MRI but is poorly delineated on standard CT, which primarily shows the gland as a uniform soft-tissue signal without clear internal zones, a common issue highlighted throughout this review.

2.2 Variations and Grading of Prostate Cancer

The overwhelming majority (>95%) of prostate malignancies are acinar adenocarcinomas; rarer histologies include ductal adenocarcinoma, neuroendocrine/small-cell carcinoma, and sarcomas. Histopathological grading uses the Gleason scoring system, in which the two most prevalent architectural patterns are each assigned a grade (3-5) and summed (e.g., 3+4=7). This has now been consolidated into the five-tier ISUP Grade Group system (Grade Group 1 = Gleason ≤6, through Grade Group 5 = Gleason 9-10) [71].

2.3 TNM Staging

Clinical and pathological staging adhere to the AJCC/UICC TNM system, in which T indicates local tumour size (T1-T4), N indicates regional lymph node involvement, and M indicates distant metastasis. Imaging techniques such as MRI are used for local (T) staging, PSMA PET/CT for assessing nodal (N) and distant (M) disease, and CT serves as an accessible, though less sensitive, alternative for evaluating gross nodal and skeletal regions, each of which contributes to the overall staging process.

2.4 Risk Factors and Screening

Risk factors include older age, family history or germline variants such as BRCA2, and African ancestry. Obesity and diet show weaker, inconsistent associations. Screening remains debated: PSA screening reduces prostate cancer-specific mortality but leads to overdiagnosis and overtreatment of slow-growing tumours. This ongoing debate has fuelled interest in MRI and, to a lesser extent, CT- and PET-based risk tools that could more accurately distinguish aggressive from indolent disease [72].

3. Results and Discussion

3.1 CT Imaging for Prostate Cancer

A typical convolutional neural network (CNN) pipeline based on CT scans involves several steps: (i) acquiring either non-contrast or contrast-enhanced helical CT images of the pelvis, often within a PET/CT study; (ii) preprocessing that includes applying Hounsfield unit windowing, resampling to isotropic voxel spacing, denoising (commonly with non-local means or learned filters), and correcting for bias-field or scanner differences; (iii) segmenting the prostate and surrounding organs, increasingly using U-Net-family networks instead of atlas-based approaches [16,17,21]; (iv) extracting the region of interest (ROI); (v) deriving radiomic or deep features including first-order intensity statistics, texture features such as gray-level co-occurrence or run-length, and CNN-based embeddings; and (vi) normalising intensities and features to minimise variability across different scanners and protocols, a common issue in CT research.

Table 1 summarises the comparative strengths and limitations of CT relative to MRI, PSMA PET/CT, ultrasound, and mpMRI for prostate cancer applications, synthesised from the reviewed literature.

Table 1. Summary comparison of imaging modalities for the diagnosis and staging of prostate carcinoma

Modality	Key strengths	Key limitations	Primary clinical role
CT	Wide availability, low	Poor soft-tissue contrast;	Segmentation of organs/OARS,

(plain/contrast)	cost, fast acquisition, and essential for RT planning	unreliable direct tumor visualization; ionizing radiation	support for staging, and risk stratification using radiomics.
MRI (T2W/DWI/DCE, mpMRI)	Superior soft-tissue and zonal contrast; PI-RADS-guided targeted biopsy; no ionizing radiation	Higher cost, longer scan time, limited availability, contraindications (implants)	Primary lesion detection, local (T) staging, active surveillance monitoring
PSMA PET/CT	High sensitivity for nodal/metastatic disease via PSMA-avid uptake; combines functional + limited anatomical data	Cost, tracer availability, low soft-tissue resolution of the CT component itself, false positives (e.g., ganglia)	Nodal/metastatic (N/M) staging, biochemical recurrence localization
Transrectal ultrasound (TRUS)	Low cost, real-time, biopsy guidance, elastography options	Operator-dependent, limited lesion conspicuity vs mpMRI	Biopsy guidance, adjunct classification with DL/radiomics

3.2 Fundamentals of Deep Learning

Artificial intelligence (AI) typically refers to computational systems that perform tasks associated with human intelligence. Machine learning (ML), a branch of AI, focuses on systems that identify patterns in data instead of following preset rules. Deep learning (DL), a specialised form of ML, employs multilayered artificial neural networks to learn hierarchical features directly from raw or lightly processed data, thereby reducing reliance on manual feature engineering common in traditional radiomics techniques.

A CNN's core operation is the discrete convolution of an input feature map X with a learnable kernel W.
$Y(i,j) = \Sigma_m \Sigma_n X(i+m, j+n) \cdot W(m,n) + b$
Where b is a bias term. Stacking convolutional layers with non-linear activation functions enables the network to progressively combine low-level edge and texture detectors into higher-level, task-relevant representations. Pooling operations, such as maximum or average pooling, downsample feature maps, thereby ensuring local translation invariance and reducing computational costs. The rectified linear unit (Relu), defined as $ReLU(x) = max(0,x)$, remains the predominant activation function due to its effectiveness in mitigating vanishing-gradient issues compared to sigmoid and tanh functions. Additionally, variants such as Leaky ReLU, GELU, and Swish are increasingly employed in transformer-influenced architectures.
Batch normalisation [71] normalises layer activations within each mini-batch, accelerating convergence and providing mild regularisation. Residual learning [56] introduces identity shortcut connections, $y = F(x) + x$, enabling gradients to propagate through very deep networks (e.g., ResNet-50/101) without vanishing. This design principle has been adopted by nearly all subsequent medical imaging CNNs, including U-Net variants used pervasively in the CT segmentation literature reviewed here.
Given the comparatively small size of most medical imaging cohorts (frequently well under 1,000 patients in the CT-specific literature identified in this review), transfer learning, which initialises networks with weights pretrained on large natural-image corpora (ImageNet) or on related radiological tasks, is near-universal practice and is explicitly reported in the majority of the classification studies synthesized in Section 3.5 [23,29].
Vision Transformers (ViT) [67] replace convolution with self-attention over image patches, enabling better capture of long-range spatial dependencies that convolution's local receptive fields may not handle as naturally. Swin Transformer [68] reimplements hierarchical, locality-focused computation through shifted windows, enhancing efficiency for dense prediction tasks like segmentation. Hybrid architectures that combine CNNS for local feature extraction with transformers for global context modelling are an emerging yet relatively unvalidated approach in prostate CT/MRI research.
Because CNNs are often seen as "black-box" predictors, explainable AI (XAI) methods such as Grad-CAM, Score-CAM, SHAP, LIME, and native attention maps in transformer models have been developed to visualise or quantify which input regions or features influence a prediction. Section3.7discusses this topic in detail, including documented limitations in reliability.

3.3 Review of CNN Architectures

This reviews critically the most common prostate deep learning architectures involving CT, MRI, and PET-CT. It evaluates each model's structure, benefits, limitations, computational demands, clinical significance, performance in specific applications, and suitable datasets.
Table 2 provides a critical comparison of CNN architectures discussed in the prostate CT, MRI, and PET-CT literature.

Table 2. Comparison of CNN architectures in prostate CT, MRI, and PET/CT studies

Architecture	Core design	Advantages	Disadvantages	Compute	Clinical applicability (this domain	Typical use/dataset
AlexNet [59]	5 conv + 3 FC layers, ReLU, dropout	Historic baseline; simple, fast to train	Shallow; largely superseded for medical imaging	Low	Baseline comparator only	Small 2D classification tasks
VGG16/VGG19 [58]	Uniform 3×3 conv stacks, 16/19 layers	Simple, strong transfer-learning backbone	Very large parameter count (~138M); high memory	High	Feature extraction backbone via transfer learning	2D MRI/CT slice classification
GoogLeNet/Inception [60]	Parallel multi-scale conv (inception modules)	Multi-scale feature capture; parameter-efficient vs VGG	More complex to tune	Moderate	Classification with limited data	Slice-level classification
ResNet [56]	Residual/skip connections, depths to 152 layers	Enables very deep training; strong general performance; ubiquitous backbone	Still memory-intensive at depth	Moderate-High	Widely used backbone across reviewed CT/MRI classification studies	Classification, feature extraction for radiomics-DL fusion
DenseNet [57]	Dense inter-layer connectivity, feature reuse	Parameter-efficient; strong gradient flow; good with limited data	High memory for activations	Moderate	Prostate zonal segmentation (DenseNet-inspired) [17]	Segmentation and classification
MobileNet [61]	Depthwise-separable convolutions	Lightweight; suitable for edge/point-of-care deployment	Lower accuracy ceiling than larger nets	Low	Deployment-constrained settings	Rapid triage classification
EfficientNet [62]	Compound scaling of depth/width/resolution	Strong accuracy-efficiency trade-off; used directly in mpMRI PCa classifiers [23]	Scaling rules less validated for volumetric medical data	Moderate	mpMRI PCa classification (reported 88.89% accuracy) [23]	2D/2.5D classification
U-Net [63]	Encoder-decoder with skip connections	De facto standard for medical segmentati	2D variant ignores inter-slice context	Moderate	Dominant architecture across the	Prostate/OAR segmentation on CT

		on; strong with limited annotated data			CT/CBCT segmentation literature reviewed [14-21]	
UNet++ [65]	Nested, dense skip pathways	Improved multi-scale feature fusion vs vanilla U-Net	Higher computational cost	Moderate-High	Boundary-sensitive segmentation tasks	Prostate gland/zonal segmentation
Mask R-CNN [66]	Region proposal + per-instance mask prediction	Simultaneous detection + instance segmentation; used for MRI lesion detection [22]	Slower inference; complex two-stage pipeline	High	Lesion-level detection tasks	mpMRI lesion detection (P5, prostatitis) [22]
nnU-Net [70]	Self-configuring U-Net variant (2D/3D/cascade)	Minimal manual tuning; state-of-the-art on many segmentation benchmarks; used directly in reviewed CT/PET-CT studies [8,21]	Long training time for 3D cascade	High	Current reference standard for CT-based organ/lesion segmentation	CT, CBCT, PET/CT segmentation
Vision Transformer (ViT) [67]	Patch-based self-attention	Captures long-range dependencies; strong with large pretraining data	Data-hungry; less mature for small medical cohorts	High	Emerging, limited validation in prostate CT literature	Large multicentre datasets
Swin Transformer [68]	Hierarchical shifted-window attention	Efficient dense prediction; competitive with CNNs on segmentation	Implementation complexity	High	Emerging use in medical segmentation benchmarks	Volumetric segmentation
ConvNeXt [69]	Modernized pure-CNN design inspired by ViT training recipes	Competitive with transformers while retaining CNN efficiency	Newer; limited prostate-specific validation	Moderate-High	Not yet widely reported in prostate CT/MRI literature	General classification backbone

Table 2 reveals a clear trend: encoder-decoder U-Net variants- such as plain U-Net, Attention U-Net, UNet++,

and especially nnU-Net- dominate the CT-specific research literature because their primary focus is segmentation rather than classification. Conversely, classification-focused backbones like ResNet, EfficientNet, DenseNet, and VGG are predominantly found in MRI and ultrasound studies, where the main goal involves diagnostic classification. This asymmetry is a significant yet often overlooked insight: CNNs are not ineffective for CT lesion classification; rather, few sufficiently large, well-powered CT classification studies have histopathological ground truth, a topic elaborated in Sections 3.10 and 3.11.

3.4 Public Datasets

Table 3 highlights the lack of a large, standardised CT-specific diagnostic dataset linked with histopathology, a notable gap in the current literature.

Table 3. Public datasets relevant to prostate CT and histopathology-linked research

Dataset	Modality	Description	Key limitations
TCIA (The Cancer Imaging Archive) [37]	Multi	Repository of numerous prostate-related collections (CT, MRI, PET/CT) across institutions	Heterogeneous annotation quality and protocols across sub-collections
PROSTATEx / PROSTATEx-2 [35]	mpMRI	204 patients, T2W/DWI/ADC/DCE, lesion centroids from SPIE-AAPM-NCI challenge	No native voxel-level gland masks in public release; extensions required [40]
PROMISE12 [34]	MRI (T2W)	50 training + additional test volumes, multi-centre, whole-gland segmentation ground truth	Whole-gland only, no zonal or lesion-level annotation; modest size
Medical Segmentation Decathlon (Prostate task) [36]	MRI (T2W+ADC)	32 training cases with peripheral/transition zone labels	Small; two-channel input limits generalizability testing
PI-CAI [39]	Biparametric MRI	~10,000 cases across public/private components; large-scale detection challenge with AI-vs-radiologist non-inferiority study	Access tiers vary; some components restricted
NCI-ISBI 2013 [via 34]	MRI	60 T2W training volumes, multi-institution	Limited to segmentation task; superseded in scale by PI-CAI

3.5 Comprehensive Literature Review

Table 4 synthesizes representative studies from this review across CT, PSMA PET/CT, mpMRI, and ultrasound, reporting the dataset, modality, model, and quantitative performance as reported in the original publications. Studies are grouped by modality to highlight the diagnosis/segmentation asymmetry discussed above.

Table 4. summarises the main literature on prostate cancer CNN research utilising CT, PET/CT, MRI, and ultrasound from 2021 to 2026.

Study	Modality	Dataset (n)	Model	Reported performance	Critical note
Wang et al. [5]	CT (plain abdominal)	539 (461 radiology + 78 nuclear medicine)	3D U-Net multi-task (MTDL) + PSAD/age nomogram	AUC reported via ROC; outperformed single-task ResNet18 and radiomics baseline	Retrospective, single-country cohort; CT-only diagnostic study, comparatively rare in literature
Ching et al. [6]	CT (radiomics)	High-risk PCa cohort	Radiomics + clinical features	AUC 0.797 (95% CI 0.768-0.826) combined vs 0.795	Prognostic, not purely

			(RC combined model)	radiomics-only	diagnostic; modest incremental gain over radiomics alone
Zang et al. [7]	68Ga-PSMA-11 PET/CT	Retrospective PCa cohort	CNN + SVM ensemble	Predicts pathological upgrading; performance reported via AUC/ROC	PET-driven signal; CT contributes anatomical registration only
Uptake segmentation framework [9]	18F-DCFPyL PET/CT	193 scans, 2 institutions	Multi-modal decision fusion CNN	Accuracy 0.764-0.796, AUC 0.851-0.863 (internal/external)	Reasonable external validation; still single-tracer emphasis
Balagopal et al. [16]	Pelvic CT	136 patients	2D+3D U-Net/ResNeXt cascade	Dice 84-96% across prostate/bladder/femoral heads/rectum	Segmentation only; no diagnostic classification
Uncertainty-aware U-Net/VAE [14]	Planning CT	300 (primary) + 10×5-reader (secondary)	U-Net + VAE ensemble with outlier mitigation	Improved contour accuracy vs baseline U-Net (geometric metrics)	RT-planning use case; not diagnostic
Lesion detection AI (MRI) [22]	T2W + ADC-DWI MRI	153 patients	Faster R-CNN, 9 classifiers	Accuracy 90-99% across sequences/classes	Small cohort; wide confidence intervals reflect this
Mehmood et al. [23]	mpMRI	Public MRI cohort	EfficientNet (transfer learning)	Accuracy 88.89%	Single-centre-style public data; limited external validation reported
T2WI Gleason prediction [24]	T2W MRI	195 controls + 302 PCa, multicentre + external	DL detection/grading model	AUC 0.918 (detection, validation set)	Multicentre and externally validated — comparatively strong methodology
Cuocolo et al. [27]	mpMRI	371 + external cohorts	Fully convolutional 3D CNN vs radiomics	Validated head-to-head against radiomics; comparable discrimination	Direct DL-vs-radiomics comparison, useful benchmark study
Huang et al. [29]	TRUS	1,380 PCa / 1,530 BPH images	7 CNN architectures + transfer learning	Comparative accuracy across architectures (best-performing models highlighted)	Ultrasound-specific; operator-dependent acquisition
Liu et al. [30]	Biparametric ultrasound + SWE	232 participants	DL radiomics + nomogram	AUC 0.80 (95% CI 0.70-0.91)	Modest external validity; single-institution

This synthesis is characterised by two main patterns. First, most studies covering CT, PET/CT, and MRI feature relatively small sample sizes, generally between 100 and 600 patients. Although some strong examples include multicentre external validation (e.g., [24,27,39]), such validation remains uncommon. Second, the reporting of performance metrics is inconsistent: some studies present only accuracy, while others present only AUC or Dice scores. Additionally, confidence intervals are often missing, which hampers cross-study comparisons and constitutes a methodological weakness in the field, as discussed further in Section 3.10.

3.6 Comparison of Performance Across Different Modalities

Direct architecture-vs-architecture benchmarking on identical prostate CT cohorts is rare in the published literature; most reviewed studies compare a proposed model against a single classical baseline (radiomics or an earlier CNN) rather than a comprehensive architecture sweep. Table 5 therefore aggregates typical reported performance ranges by task and modality, rather than presenting a single leaderboard, to avoid implying false precision in comparisons across non-identical cohorts.

Table 5 presents aggregated performance ranges, stratified by task, based on the reviewed literature. These ranges reflect diverse cohorts and are not intended for direct comparison.

Table 5. Aggregated performance ranges by task and imaging modality

Task/Modality	Primary metric(s)	Typical reported range	Representative architectures
CT organ/OAR segmentation (RT planning)	Dice coefficient	0.84 - 0.96 (prostate, bladder, femoral heads)	U-Net/nnU-Net variants [16,17,21]
PSMA PET/CT lesion segmentation	Dice / precision / recall	0.68 - 0.70 (Dice, internal/external)	3D U-Net, decision-fusion CNNs [8,9]
CT-based diagnostic classification	AUC / accuracy	Reported but sparse and heterogeneous; not yet convergent	3D U-Net multi-task, radiomics-CNN fusion [5,6]
mpMRI diagnostic classification	AUC	0.80 - 0.92	EfficientNet, 3D CNN ensembles, FCN [23,24,26,27]
Ultrasound/TRUS classification	Accuracy / AUC	0.80 (radiomics-DL fusion) up to high 90s (image classification tasks)	Transfer-learning CNN ensembles [29,30]

Computational cost and parameter count are reported inconsistently in the clinical literature (in contrast to the computer vision literature, where FLOPs and parameter counts are near-mandatory). Where reported, nnU-Net's 3D cascade and nested architectures, such as UNet++, show the highest training-time and memory costs among segmentation networks, while MobileNet and EfficientNet-B0 remain the most inference-efficient classification backbones relevant considerations for eventual point-of-care or resource-limited deployment.

3.7 Explainable AI in CNN Applications for Prostate Cancer

Grad-CAM [47] generates coarse, gradient-based class-activation heatmaps that highlight image regions influencing a CNN's prediction. It has been used directly for prostate lesion localization, where the top-weighted feature map often aligns with the lesion's anatomical location, though not in all cases [45]. Score-CAM and other gradient-free methods avoid gradient noise but require more computation. SHAP [48] offers theoretically sound feature-attribution explanations based on cooperative game theory, while LIME [49] creates local surrogate models to approximate a black-box model's behaviour around a particular prediction.

A recent large-scale meta-analysis of 67 studies in radiology, pathology, and ophthalmology revealed significant variability in the fidelity of XAI methods. It showed that LIME had markedly higher fidelity (0.81) compared to SHAP (0.38) and Grad-CAM (0.54). The analysis also noted a consistent 5-7% decline in AUC performance when interpretability constraints were added to models. Additionally, SHAP explanations proved unstable under input perturbation in some fields [44]. Similarly, a study on CT-based lung cancer diagnosis found that Grad-CAM's localization sometimes failed to accurately reflect the model's true reasoning, especially in transformer-based architectures [46]. These results discourage uncritical reliance on heatmap explanations as a replacement for thorough external validation: an anatomically plausible heatmap does not necessarily confirm a model's prediction is correct.

Clinically, XAI serves three purposes in this domain: (i) building radiologist and referring-clinician trust by making CNN decisions partially interpretable; (ii) supporting quality assurance and error analysis during model development; and (iii) potentially meeting emerging regulatory expectations for explainability in AI-based medical devices. None of these purposes are well served by any single XAI method in isolation, and multi-

method triangulation (e.g., Grad-CAM plus SHAP) is increasingly recommended over reliance on any one technique.

3.8 Clinical Workflow

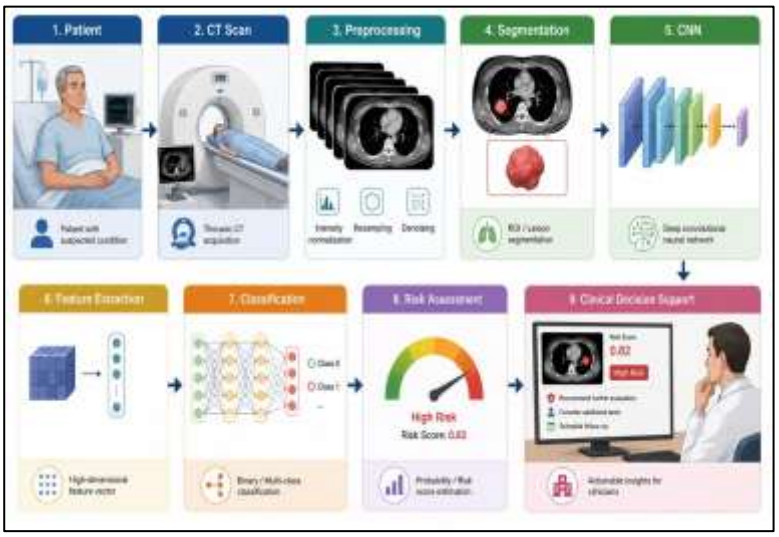

Figure 1. Workflow of the CNN-based framework for prostate cancer diagnosis using CT imaging

Figure 1 presents the overall workflow of the proposed CNN-based framework for prostate cancer diagnosis using CT imaging. The pipeline outlines the step-by-step process, starting with patient CT image acquisition, followed by preprocessing and segmentation, CNN-based feature learning and extraction, classification, risk assessment, and finally clinical decision support for prostate cancer diagnosis.

3.9 Patient Case Study

3.9.1 Case Series Rationale

Three cases from the departmental series were chosen to illustrate, using real clinical data instead of hypothetical scenarios, the main point of this review: that plain CT often cannot visually distinguish different prostatic disease states despite significant differences in pathology, digital rectal exam findings, and PSA levels. The cases are labelled only as Case 1, Case 2, and Case 3; age and sex are included because they are clinically relevant and do not reveal identities at this level of detail. Exact examination dates from the original forms are kept when clinically useful but are not linked to any personal identifiers. All three cases underwent plain (non-contrast) pelvic CT scans as part of routine care, reflecting the resource-limited, MRI-scarce setting that influences much of the CT-CNN research discussed in Sections 3.1 and 3.10.

3.9.2 Case Descriptions

Case 1 (male, 60 years). Documented history of transurethral resection of the prostate (TURP) and bilateral orchiectomy for histologically confirmed adenocarcinoma of the prostate, with subsequently rising PSA. Digital rectal examination revealed a hard prostate with pelvic side-wall infiltration by tumour, consistent with locally advanced or recurrent disease. Serum PSA was 35.57 ng/ml. Transrectal ultrasound was not performed. Plain CT of the pelvis reported the prostate as normal in size, with no focal mass described. Histopathological grade, current treatment, and outcome beyond the orchiectomy/TURP history were not recorded in the available proforma.

Case 2 (male, 21 years). Presented with back pain. Physical and digital rectal examinations were normal. Plain CT reported the prostate as normal in size, with no focal abnormality. PSA was not recorded, and no diagnosis of prostatic disease was documented; this case functions as a negative/incidental comparator, imaged for an indication unrelated to prostate cancer.

Case 3 (male, 86 years). Clinically documented as advanced-stage prostate carcinoma with a rising PSA trend. Digital rectal examination revealed a hard prostate. Serum PSA was 6.8 ng/mL at the time of imaging. Plain pelvic CT reported the prostate as normal. The combination of a clinically advanced-disease label, a comparatively modest PSA value, and an unremarkable CT is noted as an apparent discordance in the source record; whether this reflects prior androgen-deprivation therapy, a labelling inconsistency, or a genuine biological outlier cannot be determined from the available proforma.

3.9.3 Representative Imaging

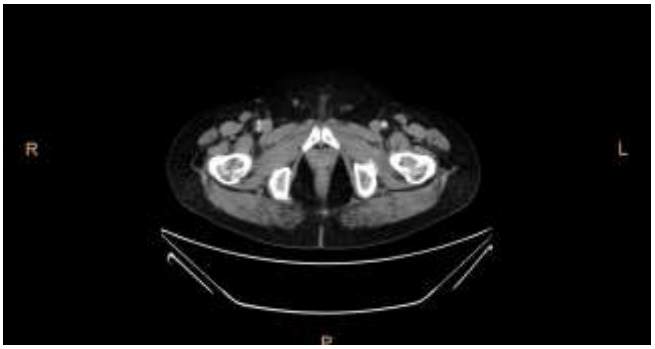

Figure 2. Case 1, plain pelvic CT (contrast-enhanced), axial section at the level of the femoral heads. Patient identifiers, hospital name, and scan date/time have been cropped from the image; orientation markers (R, L, P) are retained. The gland region shows no discretely marginated soft-tissue mass, despite the DRE and PSA findings described in Section 3.9.2, consistent with CT's limited soft-tissue contrast (Section 3.1).

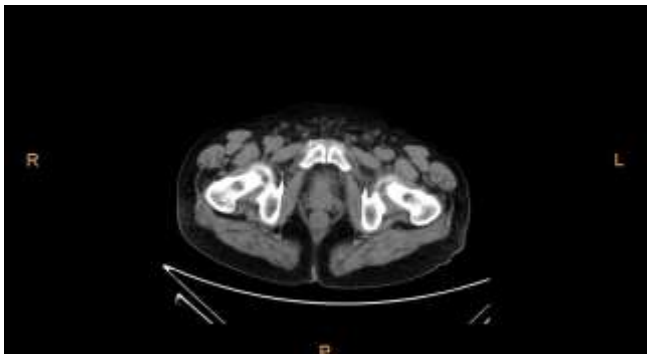

Figure 3. Case 3, plain pelvic CT, axial section at a comparable pelvic level. Patient identifiers, hospital name, and scan date/time have been cropped from the image; orientation markers (R, L, P) are retained. Despite the clinical diagnosis of advanced prostate carcinoma and a hard prostate on digital rectal examination (Section 3.9.2), no discrete focal lesion is visually apparent, consistent with the rationale for radiomic/deep-feature (rather than purely visual) analysis in CT-based pipelines.

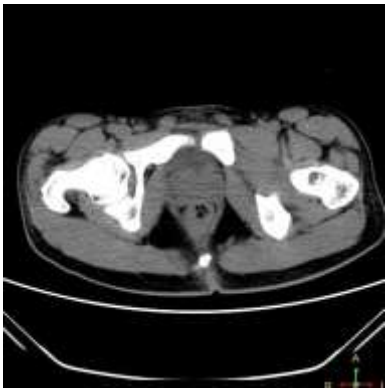

Figure 4. Case 2, plain pelvic CT, axial section. Patient identifiers, hospital name, and scan date/time have been cropped from the image; a small orientation marker (A, R) is retained. Consistent with normal physical and digital rectal examination findings and the absence of any prostatic diagnosis in this patient (Section 3.9.2), no focal abnormality is identified. This image serves as the negative/incidental comparator referenced throughout Section 3.9.

3.9.4 Rationale for Imaging and Proposed CNN Pipeline

As shown, the prostate gland does not appear as a distinct hyperdense or hypodense focal abnormality in the CT images for Cases 1-3 (Figures 2-4). This pattern aligns with the CT findings reported in Section 3.9.2 for these cases, none of which identified a discrete prostatic mass, despite two of the three being diagnosed with malignant disease clinically. This observation is intentional and informative, emphasising why CNN-based CT analysis depends on segmentation-guided radiomic and deep-feature extraction (Sections 3.9.2) instead of relying solely on visual lesion detection. It also explains why CT alone is rarely used as a primary diagnostic tool for tumor characterization (Section 3.1).

A hypothetical CNN pipeline for cases such as these would: (i) segment the prostate and pelvic organs at risk

using a U-Net/nnU-Net backbone; (ii) extract radiomic and CNN-derived deep features from the segmented regions; (iii) generate a quantitative risk score using a trained classifier; and (iv) present this score, together with Grad-CAM or SHAP overlays, to the radiologist for correlation with PSA, clinical findings, and where available MRI or PSMA PET/CT.

3.9.5 Histopathology, Staging, Treatment, and Outcomes

For Case 1, only antecedent surgical history (TURP and bilateral orchiectomy) was recorded, without a current Gleason score, TNM stage, or documented outcome.

3.9.6 Case Series Interpretation

This small case series emphasises a key point of the review: CT's role in prostate cancer diagnosis is mainly in structural segmentation for radiotherapy, staging support alongside PET, and radiomic/deep-feature pipelines. Currently, MRI and PSMA PET/CT outperform CT in detecting primary lesions (see Tables 1 and 5). Case 3 is particularly instructive: despite clinical signs of advanced prostate cancer, a hard prostate on digital rectal exam, and rising PSA levels, the CT was normal. Similarly, case 1 shows a comparable pattern post-orchiectomy, with biochemical and exam evidence of recurrent or persistent disease despite an unremarkable CT report. Case 2 involves a young patient scanned for unrelated reasons, with no clinical suspicion of prostate disease, serving as a negative comparator. These three retrospectively collected cases from a single department, with some data missing (Section 3.9.5), cannot determine diagnostic sensitivity or specificity. Their primary value is illustrative and hypothesis-generating, aligning with the structural gap in adequate CT-based diagnostic studies noted in Table 4 and discussed further in Section 3.10.

3.10 Challenges

Most CT-specific studies in this review (see Table 4) involve fewer than 600 patients, which limits their statistical power and ability to be generalised.

- Annotation burden and inter-observer variability: expert contouring of the prostate and lesions is time-consuming and inconsistent, especially on CT scans where boundaries are often ambiguous.
- Domain shift caused by differences in scanner, protocol, and reconstruction-kernel among institutions reduces model performance on external data, a limitation noted even in well-validated studies [9].
- Class imbalance: benign, indolent, and clinically significant disease are unevenly represented across most cohorts, biasing models towards the majority class.
- Most reviewed studies do not include authentic external validation across multiple institutions, with PI-CAI [39] being a notable exception.
- Explainability limitations: as detailed in Section 3.7, current XAI methods exhibit inconsistent fidelity and stability, undermining their use as the sole basis for clinical trust.
- Computational cost: 3D nnU-Net cascades and transformer-based models require significant training and inference resources, making deployment more challenging in low-resource environments.
- Regulatory approval: CT-based diagnostic (as opposed to segmentation) AI tools for prostate cancer remain largely investigational, with few, if any, achieving the level of clinical validation of comparable MRI-based commercial tools [42].
- Clinical adoption and workflow integration: radiologists' trust, medico-legal liability, and integration with existing PACS/RIS workflows remain practical barriers beyond model performance alone.
- Ethical issues, privacy, and data security: Sharing data across institutions for larger CT cohorts raises concerns about patient privacy and data governance, leading to increased interest in federated learning (Section 3.11).

3.11 Future Research Directions

- Federated learning: enabling multi-institutional model training on CT/MRI data without centralising patient images, directly addressing the small-dataset and privacy challenges [50-55].
- Foundation models and vision-language models: large, self-supervised, pre-trained imaging models (and image-text models incorporating radiology reports) may reduce reliance on large labelled CT cohorts.
- Multimodal AI: integrated modelling of computed tomography (CT), magnetic resonance imaging (MRI), PSMA positron emission tomography (PET), clinical variables (including PSA levels and age), as well as histopathology and genomics, to enhance diagnostic and prognostic precision surpassing that achievable by any individual modality.
- Self-supervised and few-shot learning: pretext-task pretraining on unlabelled CT volumes to reduce the annotation burden, particularly relevant given the scarcity of labelled data identified throughout this review.
- Synthetic data generation: using generative models (GANs, diffusion models) to augment small CT cohorts and address class imbalance, with appropriate caution regarding the validity of synthetic data.
- Enhanced, quantitatively validated explainable AI: advancing from qualitative heatmaps to fidelity- and stability-benchmarked XAI, in line with recent meta-analyses [43].
- Real-time or near-real-time diagnosis: computationally efficient architectures (MobileNet/EfficientNet-class

models) suitable for point-of-care or intraoperative deployment.
• Digital twins and personalized medicine involve patient-specific modelling that combines imaging, treatment response, and outcome data to tailor therapy choices.
• Prospective, multicentre clinical deployment studies: the field currently lacks prospective trials analogous to PI-CAI [39] for CT-based diagnostic tools; this is arguably the top-priority gap.
Summarising the previous sections, three key points emerge. First, the CT-specific literature on prostate cancer mainly focuses on segmentation rather than diagnosis, due to CT's limited soft-tissue contrast, not a lack of research. Therefore, it is probably incorrect to see future CT-CNN work as competing with MRI for primary lesion detection. Instead, it is more supported to view this work as complementary, especially for staging, radiotherapy planning, and radiomic risk stratification, as shown in Tables 4 and 5.
Second, methodological rigor is uneven across the reviewed literature. Reporting of confidence intervals, external validation, and standardised metrics (Dice, AUC with CI, sensitivity/specificity at defined operating points) is inconsistent, which itself is a barrier to meta-analysis and regulatory evaluation. Studies such as the T2WI multicentre Gleason-prediction study [24] and the PI-CAI trial [39] set the methodological standard the field should converge towards, but remain the exception rather than the norm, particularly for CT-specific work.
Third, even within narrow sub-domains, contradictory results are evident. For instance, XAI fidelity scores can differ by several times across methods and modalities within the same meta-analysis [44]. Additionally, segmentation Dice scores show significant variation (0.68-0.96) based on the structure, modality, and validation setting (see Table 5). This highlights that performance figures from single studies should not be overgeneralized. Clinically, this suggests that CT-based CNN tools should currently serve as decision-support aids within a broader multimodal approach involving PSA, MRI, PSMA PET/CT, and histopathology, rather than replacing diagnostics autonomously. Furthermore, clinicians and journal reviewers should require external validation and confidence intervals before accepting reported performance metrics unquestioningly.

4. Conclusion

Convolutional neural networks have significantly advanced CT-based image analysis for prostate cancer, mainly aiding organ and target-volume auto-segmentation in radiotherapy planning and supporting PSMA PET/CT interpretation. However, they have not yet replaced standalone diagnostic classification, where MRI approaches remain more developed and validated. This gap reflects a real physical limitation of CT, not a research oversight, and should influence how future work is approached and assessed. Ongoing challenges such as small, heterogeneous datasets, inconsistent external validation, unresolved explainability issues, and regulatory hurdles must be addressed through larger multicenter CT datasets linked to histopathology, standardized performance reporting, federated and self-supervised learning, and rigorously validated explainable AI. Responsible deployment of CT-based CNN diagnostic tools will likely involve their integration into multimodal diagnostic and staging workflows, rather than replacing MRI or PSMA PET/CT in the near term.

Acknowledgement: The authors thank the patients and their family for providing clinical information and consent for publication. We also acknowledge the clinical team for their support.

Funding Information: The authors received no specific funding for this study.

Conflict of Interest: The authors declare that they have no conflict of interest.

Author's contribution: B. Manju: Conceptualization, data collection, and manuscript preparation. J. Asha: Clinical assessment, data interpretation, and manuscript review.

Soumya Varma: Literature review, data analysis, and manuscript editing. Ajay James: Supervision, critical revision, and final approval of the manuscript. All authors read and approved the final manuscript.

Other Ethics Statements: The case report was prepared in accordance with applicable ethical standards.

References

1. Sung H, Ferlay J, Siegel RL, Laversanne M, Soerjomataram I, Jemal A, et al. Global cancer statistics 2020: GLOBOCAN estimates of incidence and mortality worldwide for 36 cancers in 185 countries, CA Cancer J Clin, 71(3) (2021) 209-249. https://doi.org/10.3322/caac.21660
2. Siegel RL, Miller KD, Fuchs HE, Jemal A, Cancer statistics, 2022, CA Cancer J Clin, 72(1) (2022) 7-33. https://doi.org/10.3322/caac.21708
3. Siegel RL, Miller KD, Fuchs HE, Jemal A, Cancer statistics, 2021, CA Cancer J Clin, 71(1) (2021) 7-33. https://doi.org/10.3322/caac.21654
4. Litjens G, Kooi T, Bejnordi BE, Setio AAA, Ciompi F, Ghafoorian M, et al., A survey on deep learning in

medical image analysis, Med Image Anal, 42 (2017) 60-88. https://doi.org/10.1016/j.media.2017.07.005
5. Wang Y, Zhang F, Chen X, Zhang X, Zhu H, He X, et al. Significance of multi-task deep learning neural networks for diagnosing clinically significant prostate cancer in plain abdominal CT, Quant Imaging Med Surg, 15(5) (2025). https://doi.org/10.3389/fonc.2025.1543230
6. Ching CBB, Lam WWC, Lam TC, Lui AKY, Kwong DLW, Lo AWI, et al. Integrating CT-based radiomic model with clinical features improves long-term prognostication in high-risk prostate cancer, Front Oncol, 13 (2023) 1060687. https://doi.org/10.3389/fonc.2023.1060687
7. Zang S, Jiang C, Zhang W, Fu J, Meng W, Wu H, et al. Deep learning based on 68Ga-PSMA-11 PET/CT for predicting pathological upgrading in patients with prostate cancer, Front Oncol, 13 (2024) 1273414. https://doi.org/10.3389/fonc.2023.1273414
8. Qiu RLJ, Chang C-W, Yang X. Deep learning-assisted lesion segmentation in PET/CT imaging: A feasibility study for salvage radiation therapy in prostate cancer, Oncoscience, 11 (2024) 31-40.
9. Automated deep learning-based framework for uptake segmentation and classification on PSMA PET/CT imaging of patients with prostate cancer, J Imaging Inform Med (2024).
10. Panteleimonitis S, et al. Dual channel CW nnU-Net for 3D PET-CT lesion segmentation in the 2024 autoPET III challenge, arXiv (2024).
11. Capobianco N, Shah V, Spottiswoode B, Thiessen J, Bauman G. miTNM nodal and metastatic prostate cancer staging using deep learning in 68Ga-PSMA-11 and 18F-DCFPyL PET/CT, J Nucl Med, 64(Suppl 1) (2023) P447.
12. Huang B, Yang Q, Li X, Wu Y, Liu Z, Pan Z, et al. Deep learning-based whole-body characterization of prostate cancer lesions on [68Ga]Ga-PSMA-11 PET/CT in patients with post-prostatectomy recurrence, Eur J Nucl Med Mol Imaging, 51(4) (2024) 1173-1184. https://doi.org/10.1007/s00259-023-06551-3.
13. Holzschuh JC, Mix M, Ruf J, Hölscher T, Kotzerke J, Vrachimis A, et al. Deep learning based automated delineation of the intraprostatic gross tumour volume in PSMA-PET for patients with primary prostate cancer, Radiother Oncol, 188 (2023) 109774. https://doi.org/10.1016/j.radonc.2023.109774.
14. Li X, Bagher-Ebadian H, Gardner S, Kim J, Elshaikh MA, Movsas B, et al. An uncertainty-aware deep learning architecture with outlier mitigation for prostate gland segmentation in radiotherapy treatment planning, Med Phys, 50(1) (2023) 311-322.
15. Kawula M, Purice D, Li M, Vivar G, Ahmadi SA, Parodi K, et al. Dosimetric impact of deep learning-based CT auto-segmentation on radiation therapy treatment planning for prostate cancer, Phys Imaging Radiat Oncol, 17 (2022) 21. https://doi.org/10.1186/s13014-022-01985-9
16. Balagopal A, Kazemifar S, Nguyen D, Lin M-H, Hannan R, Owrangi A, et al. Fully automated organ segmentation in male pelvic CT images, Phys Med Biol, 63(24) (2018) 245015. https://doi.org/10.1088/1361-6560/aaf11c
17. Erdur AC, Rusche D, Scholz D, Kiechle J, Fischer S, Llorián-Salvador Ó, et al. Deep learning for autosegmentation for radiotherapy treatment planning: state-of-the-art and novel perspectives, Strahlenther Onkol, 201(3) (2025) 236-254. https://doi.org/10.1007/s00066-024-02262-2
18. Nemoto T, Futakami N, Yagi M, Kunieda E, Akiba T, Takeda A, Shigematsu N. Simple low-cost approaches to semantic segmentation in radiation therapy planning for prostate cancer using deep learning with non-contrast planning CT images, Phys Med, 78 (2020) 93-100. https://doi.org/10.1016/j.ejmp.2020.09.004
19. Brioso RC, Dei D, Franzese C, Lambri N, Loiacono D, Mancosu P, Scorsetti M. Segmentation of planning target volume in CT series for total marrow irradiation using U-Net, arXiv (2023). https://doi.org/10.48550/arXiv.2304.02353
20. Abbani N, Baudier T, Rit S, Franco FD, Okoli F, Jaouen V, Tilquin F, Barateau A, Simon A, de Crevoisier R, Bert J, Sarrut D. Deep learning-based segmentation in prostate radiation therapy using Monte Carlo simulated cone-beam computed tomography, Med Phys, 49(11) (2022) 6930-6944. https://doi.org/10.1002/mp.15946
21. Mofid B, Mosalla SMM, Goodarzi M, Tavakoli H. Deep CNN-based fully automated segmentation of pelvic multi-organ on CT images for prostate cancer radiotherapy, J Biomed Phys Eng, 15(6) (2025) 575-588. https://doi.org/10.31661/jbpe.v0i0.2307-1649
22. Kaya M, Durdag O, Solak M, Coskuncay A, Burakgazi G. Lesion detection using artificial intelligence models in MR images of prostate cancer and prostatitis patients and comparison of model performance, Front Urol, 5 (2026) 1726795. https://doi.org/10.3389/fruro.2025.1726795
23. Mehmood M, Abbasi SH, Aurangzeb K, Majeed MF, Anwar MS, Alhussein M. A classifier model for prostate cancer diagnosis using CNNs and transfer learning with multi-parametric MRI, Front Oncol, 13 (2023) 1225490. https://doi.org/10.3389/fonc.2023.1225490
24. Jin L, Yu Z, Gao F, Li M, et al. T2-weighted imaging-based deep-learning method for noninvasive

prostate cancer detection and Gleason grade prediction: a multicenter study, Insights Imaging, 15 (2024) 111. https://doi.org/10.1186/s13244-024-01682-z
25. Cipollari S, Guarrasi V, Pecoraro M, Bicchetti M, Messina E, Farina L, et al. Convolutional neural networks for automated classification of prostate multiparametric magnetic resonance imaging based on image quality, J Magn Reson Imaging, 55(2) (2022) 480-490. https://doi.org/10.1002/jmri.27879
26. Yi Z, Ou Z, Hu J, Qiu D, Quan C, Othmane B, Wang Y, Wu L. Computer-aided diagnosis of prostate cancer based on deep neural networks from multi-parametric magnetic resonance imaging, Front Physiol, 13 (2022) 918381. https://doi.org/10.3389/fphys.2022.918381
27. Castillo T JM, Arif M, Starmans MPA, Niessen WJ, Bangma CH, Schoots IG, Veenland JF. Classification of clinically significant prostate cancer on multi-parametric MRI: a validation study comparing deep learning and radiomics, Cancers (Basel), 14(1) (2022) 12. https://doi.org/10.3390/cancers14010012
28. Saunders S, Rusu M, Sonn G, Iagaru A. Improving prostate cancer detection from MRI with ensembled deep learning models [seminar], Stanford SCIT Program (2023).
29. Huang TL, Lu NH, Huang YH, Twan WH, Yeh LR, Liu KY, et al. Transfer learning with CNNs for efficient prostate cancer and BPH detection in transrectal ultrasound images, Sci Rep, 13 (2023) 21849. https://doi.org/10.1038/s41598-023-49159-1
30. Liu X, Zhang ZX, Zheng B, Xu M, Cao XY, Huang HM. A retrospective study on predicting clinically significant prostate cancer via a bi-parametric ultrasound-based deep learning radiomics model, Front Oncol, 15 (2025) 1538854. https://doi.org/10.3389/fonc.2025.1538854
31. Zhang YF, Zhou C, Guo S, Wang C, Yang J, Yang ZJ, et al. Deep learning algorithm-based multimodal MRI radiomics and pathomics data improve prediction of bone metastases in primary prostate cancer, J Cancer Res Clin Oncol, 150(2) (2024) 78. https://doi.org/10.1007/s00432-023-05574-5
32. Zheng B, Mo F, Shi X, Li W, Shen Q, Zhang L, et al. An automatic deep-radiomics framework for prostate cancer diagnosis and stratification in patients with serum prostate-specific antigen of 4.0-10.0 ng/mL: a multicenter retrospective study, Acad Radiol, 32(5) (2025) 2709-2722. https://doi.org/10.1016/j.acra.2024.12.012
33. Olawuyi O, Viriri S. Deep learning techniques for prostate cancer analysis and detection: survey of the state of the art, J Imaging, 11(8) (2025) 254. https://doi.org/10.3390/jimaging11080254
34. Litjens G, Toth R, van de Ven W, Hoeks C, Kerkstra S, van Ginneken B, et al. Evaluation of prostate segmentation algorithms for MRI: the PROMISE12 challenge, Med Image Anal, 18(2) (2014) 359-373
35. Armato SG, Huisman H, Drukker K, Hadjiiski L, Kirby JS, Petrick N, et al. PROSTATEx challenges for computerized classification of prostate lesions from multiparametric magnetic resonance images, J Med Imaging (Bellingham), 5(4) (2018) 044501. https://doi.org/10.1117/1.JMI.5.4.044501
36. Antonelli M, Reinke A, Bakas S, Farahani K, Kopp-Schneider A, Landman BA, et al. The Medical Segmentation Decathlon, Nat Commun, 13 (2022) 4128. https://doi.org/10.1038/s41467-022-30695-9
37. Clark K, Vendt B, Smith K, Freymann J, Kirby J, Koppel P, et al. The Cancer Imaging Archive (TCIA): maintaining and operating a public information repository, J Digit Imaging, 26(6) (2013) 1045-1057. https://doi.org/10.1007/s10278-013-9622-7
38. Cuocolo R, Comelli A, Stefano A, Benfante V, Dahiya N, Stanzione A, et al. Deep learning whole-gland and zonal prostate segmentation on a public MRI dataset, J Magn Reson Imaging, 54(2) (2021) 452-459.
39. Saha A, Bosma JS, Twilt JJ, van Ginneken B, Bjartell A, Padhani AR, et al. Artificial intelligence and radiologists in prostate cancer detection on MRI (PI-CAI): an international, paired, non-inferiority, confirmatory study, Lancet Oncol, 25(7) (2024) 879-887.
40. KLO-Net: a dynamic K-NN attention U-Net with CSP encoder for efficient prostate gland segmentation from MRI, arXiv (2025). https://doi.org/10.48550/arXiv.2512.13902
41. Innocenti L, et al. Benchmarking collaborative learning methods for prostate segmentation across heterogeneous imaging centers, arXiv (2023). https://doi.org/10.48550/arXiv.2309.17097
42. van der Leest M, Cornel E, Israel B, Hendriks R, Padhani AR, Hoogenboom M, et al. Artificial intelligence for prostate MRI: open datasets, available applications, and grand challenges, Eur Radiol Exp, 6 (2022) 35.
43. Enhancing interpretability in brain tumor detection: leveraging Grad-CAM and SHAP for explainable AI in MRI-based cancer diagnosis, ResearchGate (2026).
44. Beyond post hoc explanations: a comprehensive framework for accountable AI in medical imaging through transparency, interpretability, and explainability, NPJ Digit Med (2025).
45. Exploring the explainability of a machine learning model for prostate cancer: do lesions localize with the most important feature maps?, medRxiv (2024). https://doi.org/10.1101/2024.10.12.24315347
46. Panboonyuen T. Seeing isn't always believing: analysis of Grad-CAM faithfulness and localization

reliability in lung cancer CT classification, arXiv (2026). https://doi.org/10.48550/arXiv.2601.12826
47. Selvaraju RR, Cogswell M, Das A, Vedantam R, Parikh D, Batra D. Grad-CAM: visual explanations from deep networks via gradient-based localization, Int J Comput Vis, 128 (2020) 336-359.
48. Selvaraju RR, Cogswell M, Das A, Vedantam R, Parikh D, Batra D. Grad-CAM: visual explanations from deep networks via gradient-based localization, Int J Comput Vis, 128 (2020) 336-359.
49. Ribeiro MT, Singh S, Guestrin C. "Why should I trust you?": explaining the predictions of any classifier, Proc 22nd ACM SIGKDD Int Conf Knowl Discov Data Min (2016) 1135-1144.
50. SelfFed: self-supervised federated learning for data heterogeneity and label scarcity in medical images, Expert Syst Appl (2024).
51. Linardos A, Pati S, Baid U, Edwards B, Foley P, Ta K, et al. The MICCAI Federated Tumor Segmentation (FeTS) Challenge 2024: efficient and robust aggregation methods for federated learning, arXiv (2025). https://doi.org/10.48550/arXiv.2512.06206
52. Advancements and challenges of federated learning in medical imaging: a systematic literature review, Artif Intell Rev (2026).
53. Federated learning for medical image analysis: privacy-preserving paradigms and clinical challenges, 2025.
54. Technical and legal aspects of federated learning in bioinformatics: applications, challenges and opportunities, arXiv (2025). https://doi.org/10.48550/arXiv.2503.09649
55. McMahan HB, Moore E, Ramage D, Hampson S, y Arcas BA. Communication-efficient learning of deep networks from decentralized data, Proc 20th Int Conf Artif Intell Stat, 54 (2017) 1273-1282.
56. He K, Zhang X, Ren S, Sun J. Deep residual learning for image recognition, Proc IEEE Conf Comput Vis Pattern Recognit (2016) 770-778.
57. Huang G, Liu Z, van der Maaten L, Weinberger KQ. Densely connected convolutional networks, Proc IEEE Conf Comput Vis Pattern Recognit (2017) 4700-4708.
58. Simonyan K, Zisserman A. Very deep convolutional networks for large-scale image recognition, arXiv (2014). https://doi.org/10.48550/arXiv.1409.1556.
59. Krizhevsky A, Sutskever I, Hinton GE. ImageNet classification with deep convolutional neural networks, Adv Neural Inf Process Syst, 25 (2012) 1097-1105.
60. Szegedy C, Liu W, Jia Y, Sermanet P, Reed S, Anguelov D, et al. Going deeper with convolutions, Proc IEEE Conf Comput Vis Pattern Recognit (2015) 1-9.
61. Howard AG, Zhu M, Chen B, Kalenichenko D, Wang W, Weyand T, et al. MobileNets: efficient convolutional neural networks for mobile vision applications, arXiv (2017). https://doi.org/10.48550/arXiv.1704.04861
62. Tan M, Le Q. EfficientNet: rethinking model scaling for convolutional neural networks, Proc Int Conf Mach Learn (2019) 6105-6114.
63. Ronneberger O, Fischer P, Brox T. U-Net: convolutional networks for biomedical image segmentation, Med Image Comput Comput Assist Interv (2015) 234-241.
64. Oktay O, Schlemper J, Le Folgoc L, Lee M, Heinrich M, Misawa K, et al. Attention U-Net: learning where to look for the pancreas, arXiv (2018). https://doi.org/10.48550/arXiv.1804.03999
65. Zhou Z, Rahman Siddiquee MM, Tajbakhsh N, Liang J. UNet++: a nested U-Net architecture for medical image segmentation, Deep Learn Med Image Anal Multimodal Learn Clin Decis Support (2018) 3-11.
66. He K, Gkioxari G, Dollar P, Girshick R. Mask R-CNN, Proc IEEE Int Conf Comput Vis (2017) 2961-2969.
67. Dosovitskiy A, Beyer L, Kolesnikov A, Weissenborn D, Zhai X, Unterthiner T, et al. An image is worth 16x16 words: transformers for image recognition at scale, arXiv (2020). https://doi.org/10.48550/arXiv.2010.11929
68. Liu Z, Lin Y, Cao Y, Hu H, Wei Y, Zhang Z, et al. Swin Transformer: hierarchical vision transformer using shifted windows, Proc IEEE Int Conf Comput Vis (2021) 10012-10022.
69. Liu Z, Mao H, Wu C-Y, Feichtenhofer C, Darrell T, Xie S. A ConvNet for the 2020s, Proc IEEE Conf Comput Vis Pattern Recognit (2022) 11976-11986.
70. Isensee F, Jaeger PF, Kohl SAA, Petersen J, Maier-Hein KH. nnU-Net: a self-configuring method for deep learning-based biomedical image segmentation, Nat Methods, 18(2) (2021) 203-211.
71. Ioffe S, Szegedy C. Batch normalization: accelerating deep network training by reducing internal covariate shift, Proc Int Conf Mach Learn (2015) 448-456.
72. Bulten W, Kartasalo K, Chen P-HC, Strom P, Pinckaers H, Nagpal K, et al. Artificial intelligence for diagnosis and Gleason grading of prostate cancer: the PANDA challenge, Nat Med, 28(1) (2022) 154-163.
73. Twilt JJ, Saha A, Bosma JS, van Leeuwen KG, Bomers JGR, Huisman H, et al. Artificial intelligence based algorithms for prostate cancer classification and detection on magnetic resonance imaging: a narrative review, Diagnostics, 11(6) (2021) 959.
74. Cornford P, van den Bergh RCN, Briers E, den Broeck TVD, Cumberbatch MG, De Santis M, et al. EAU-

EANM-ESTRO-ESUR-ISUP-SIOG guidelines on prostate cancer, Eur Urol, 79(2) (2021) 243-262.
75. Kasivisvanathan V, Rannikko AS, Borghi M, Panebianco V, Mynderse LA, Vaarala MH, et al. MRI-targeted or standard biopsy for prostate-cancer diagnosis, N Engl J Med, 378(19) (2018) 1767-1777.
76. Epstein JI, Egevad L, Amin MB, Delahunt B, Srigley JR, Humphrey PA. The 2014 International Society of Urological Pathology (ISUP) Consensus Conference on Gleason Grading of Prostatic Carcinoma, Am J Surg Pathol, 40(2) (2016) 244-252.